

# Assigning $^1\text{H}$ Chemical Shifts in Paramagnetic Mono and Bimetallic Surface Sites using DFT: a Case Study on the Union Carbide Polymerization Catalyst

Anna Giorgia Nobile,<sup>[a]</sup> David Trummer,<sup>[a]</sup> Zachariah J. Berkson,<sup>[a]</sup> Michael Wörle,<sup>[a]</sup> Christophe Copéret,<sup>[a],\*</sup> Pierre-Adrien Payard<sup>[a],[b],\*</sup>

[a] *ETH Zürich Department of Chemistry and Applied Biosciences  
Vladimir-Prelog-Weg 2, CH-8093 Zürich, Switzerland*

[b] *Université de Lyon, Université Claude Bernard Lyon I, CNRS, INSA, CPE, UMR 5246, ICBMS, rue Victor Grignard, F-69622 Villeurbanne Cedex, France*

Email: [ccoperet@ethz.ch](mailto:ccoperet@ethz.ch), [pierre-adrien.payard@univ-lyon1.fr](mailto:pierre-adrien.payard@univ-lyon1.fr)

**Abstract:** The Union Carbide (UC) ethylene polymerization catalyst, based on silica-supported chromocene, is one of the first industrial catalysts prepared by surface organometallic chemistry, though the structure of the surface sites remains elusive. Recently, our group reported that monomeric and dimeric Cr (II) sites as well as Cr(III) hydride sites are present and that their proportion varies as a function of the Cr loading. While  $^1\text{H}$  chemical shifts extracted from solid-state  $^1\text{H}$  NMR spectra should be diagnostic of the structure of such surface sites, unpaired electrons centered on Cr atoms induce large paramagnetic  $^1\text{H}$  shifts that complicate NMR analysis. Here, we implement a cost-efficient DFT methodology to calculate  $^1\text{H}$  chemical shifts for antiferromagnetically coupled metal dimeric sites using a Boltzmann-averaged Fermi contact term over the population of the different spin states. This method allowed us to assign the  $^1\text{H}$  chemical shifts observed for the industrial-like UC catalyst. The presence of monomeric and dimeric Cr(II) sites as well as a dimeric Cr(III)-hydride site was confirmed and their structure was clarified.

## Introduction

Polyethylene (PE) is one of the most commonly used plastics with annual production exceeding 100 million tons.[1] Its production relies mostly on the Ziegler-Natta or Phillips catalysts, involving paramagnetic Ti(III) and Cr(III) active sites.[1-3] Another notable example is the Union Carbide (UC) catalyst, based on silica-supported chromocene  $\text{Cr}^{\text{II}}\text{Cp}_2$  (**1**), that has been used for specialized applications.[4-6] The nature of its surface and active sites has been under investigation for more than 50 years due to the complexity of this system, though various types of Cr sites have been proposed based on IR and solid-state NMR spectroscopic analyses.[5, 7-9] For example, we have recently investigated the effect of the Cr loading on the IR response after CO adsorption in the UC catalyst. Complemented with detailed computational studies, it was possible to identify mono-grafted Cr(II) sites **I** as well as dimeric Cr(II) sites with weak (**III**) and strong (**II**) Cr-Cr interactions (Fig. 1A).[10] At high Cr loading (1 and 2 wt% Cr), we reported that dimeric and monomeric Cr(III)-hydrides (**IV** and **V**) are likely present, as evidenced by the appearance of low energy CO bands, indicative of Cr-formyl species formed upon CO insertion into a Cr-hydride bond. The presence of these sites was also supported by EPR spectroscopy and labeling studies. This study also indicated that the active sites are more likely to be Cr(III) sites, consistent with what was found in the corresponding molecular systems.[11, 12]

With these results in hand, we decided to re-investigate the speciation of surface sites using solid-state NMR spectroscopy, which used in pioneering studies on understanding Cr-site speciation.[13] The advantage of this technique over IR spectroscopy is its high spectral resolution without the need for probe molecules that can influence or modify the surface site distributions and structures. However, the presence of unpaired

electrons in Cr-based sites introduces additional complexity that impedes a straightforward interpretation of NMR spectra. Indeed, the interaction of unpaired electrons with nuclear spins yields so-called paramagnetic chemical shifts that can appear in a broad range and that are impossible to predict by way of basic qualitative reasoning.[14-17] This makes the assignment of paramagnetically shifted signals exceptionally challenging, especially in the case of multimeric sites and antiferromagnetically coupled Cr atoms. While computational protocols have been optimized to calculate paramagnetic chemical shifts in the case of monomeric metal complexes,[14, 18] no work has been reported in the case of dimeric complexes from the best of our knowledge.

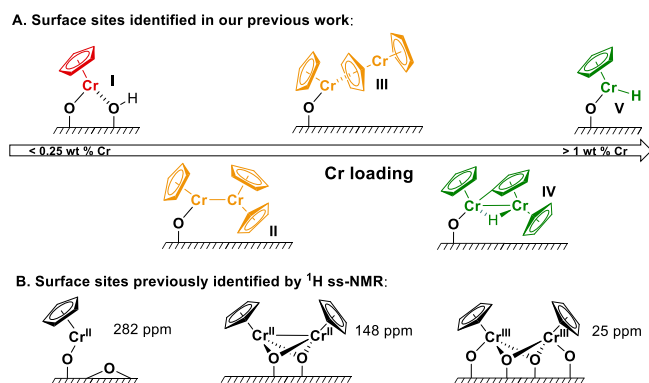


**Figure 1 A.** Identified surface sites in the UC catalyst as a function of the Cr loading based on the CO-IR and EPR spectroscopies as well as DFT studies as outlined in our previous work.[10] The numbering of the surface species has been adapted accordingly. At low Cr loading, monomeric Cr sites I are mainly present; these sites can possibly interact with residual surface OH groups (*vide infra*). When increasing the loading, site I can interact with **1** to form dimeric sites with a bridging Cp ligand (III) or direct Cr-Cr interaction (II). Site II can yield a bridging Cr(III)-hydride complex (IV) *via* C-H activation at the Cp ring, which can further react with a surface hydroxyl group leading to a monomeric Cr(III) hydride (V). **B.** A mono-grafted Cr site and dimeric Cr(III) and Cr(II) surface sites were identified by Schnellbach *et al.* using temperature-dependent  $^1\text{H}$  MAS NMR spectroscopy.[19]

Previous  $^1\text{H}$  solid-state magic-angle-spinning (MAS) NMR studies on the UC-catalyst at low Cr loading highlighted the presence of two signals consistent with surface-attached chromium species around 282 ppm and 25 ppm.[13] At higher Cr loadings it was reported that the signal intensity of the peak at 282 ppm decreases with the appearance of a new resonance at 148 ppm. Furthermore, it was reported that the signal at 282 ppm shifts to a higher chemical shift upon lowering the temperature, while the signals at 148 ppm and 25 ppm are insensitive to temperature changes.[13] Based on these findings, the signal at 282 ppm was assigned to a mono-grafted chromium site, while the resonances at 148 ppm and 25 ppm to dimeric Cr(III) and Cr(II) sites respectively (Fig. 1B).

In this work, we first investigated the effect of the Cr loading on the  $^1\text{H}$  MAS NMR signatures of **1** supported on  $\text{SiO}_{2-700}$  to parallel what we have recently carried out with IR spectroscopy.[20] Next, we optimized a computational approach to evaluate the chemical shift of weakly interacting spins in bimetallic complexes. More precisely, the chemical shift was calculated using a Boltzmann distribution of the Fermi contact terms averaged over the different spin states, calculated using a DFT methodology inspired by Rastrelli and Bagno.[14, 21] The spin-spin coupling constant  $J$ , which determines the splitting of the spin states, was estimated using the broken symmetry approach.[22] This methodology was benchmarked on a series of paramagnetic metal monomers and dimers and later on used to decipher the structure of surface sites by assigning paramagnetic-shifted  $^1\text{H}$  MAS NMR signals of the industrial-like UC-catalyst at various Cr loadings.

## Results and Discussion

### 1. $^1\text{H}$ Chemical shifts in the industrial-like UC catalyst

The industrial-like UC catalyst was prepared by reacting chromocene  $\text{CrCp}_2$  (**1**) with silica, partially dehydroxylated at  $700^\circ\text{C}$ , according to our previously reported procedure.[10] The catalyst was prepared with four different Cr loading: 0.25, 0.5, 1.0, and 2.0 wt. % of Cr, yielding respectively **1-SiO<sub>2</sub>-0.25**, **1-SiO<sub>2</sub>-0.5**, **1-SiO<sub>2</sub>-1**, and **1-SiO<sub>2</sub>-2**. The solid-state  $^1\text{H}$  MAS NMR spectra were acquired at 16.4 T (700 MHz for  $^1\text{H}$ ), in flowing dry  $\text{N}_2$  gas, and a temperature of 280 K. In addition, the temperature dependence of the NMR signals was investigated by recording spectra at 293, 273, and 253 K.  $^1\text{H}$  MAS rates of 35 and 40 kHz were used to minimize overlap of paramagnetic shifted  $^1\text{H}$  signals and spinning sidebands.[23] For each sample, three  $^1\text{H}$  MAS NMR spectra with different center frequencies of 300 ppm, 150 ppm, and 0 ppm were recorded to detect the different paramagnetic-shifted signals.

The  $^1\text{H}$  MAS NMR spectrum of **1-SiO<sub>2</sub>-1** in Figure 2 shows a substantial sideband manifold, consistent with large  $^1\text{H}$  chemical shift anisotropies associated with the paramagnetic nature of surface Cr sites.[13, 15, 24] Besides the spinning sidebands, the  $^1\text{H}$  ss-NMR spectrum of **1-SiO<sub>2</sub>-1** shows a weak, highly deshielded signal at 318 ppm, together with a more intense signal around 155 ppm. The latter disappears after long acquisition times ( $\sim$ days) regardless of the temperature of the measurement, indicating the sensitivity of the associated surface species. Besides the two highly de-shielded signals, two additional peaks close to the diamagnetic region appear at 23 ppm and 12 ppm, as previously reported.[13] In the diamagnetic region, the peaks at 2.1 and 4.3 ppm are associated with isolated and interacting OH groups of the silica surface[25] and the one at 6.7 ppm with traces amount of cyclopentadiene adsorbed on silica, similar to what is observed for pentamethylcyclopentadiene.[26]

Regarding temperature dependence, the most de-shielded peak at 318 ppm shifts downfield while cooling below room temperature ( $\Delta T = -40$  K,  $\Delta\delta = +46$  ppm). The peak at 155 ppm also shifts downfield while cooling below room temperature, but with a less pronounced temperature dependence ( $\Delta T = -40$  K,  $\Delta\delta = +16$  ppm) that is also indicative for monomeric sites as reported by Schnellbach[13] (see Fig. S6 for details). Contrary to the highly de-shielded resonances, the two peaks close to the diamagnetic region shift slightly up-field upon cooling below room temperature:  $\Delta T = -40$  K,  $\Delta\delta = -3$  (peak at 23 ppm) and  $-2$  (peak at 12 ppm) as shown in Fig. S6.

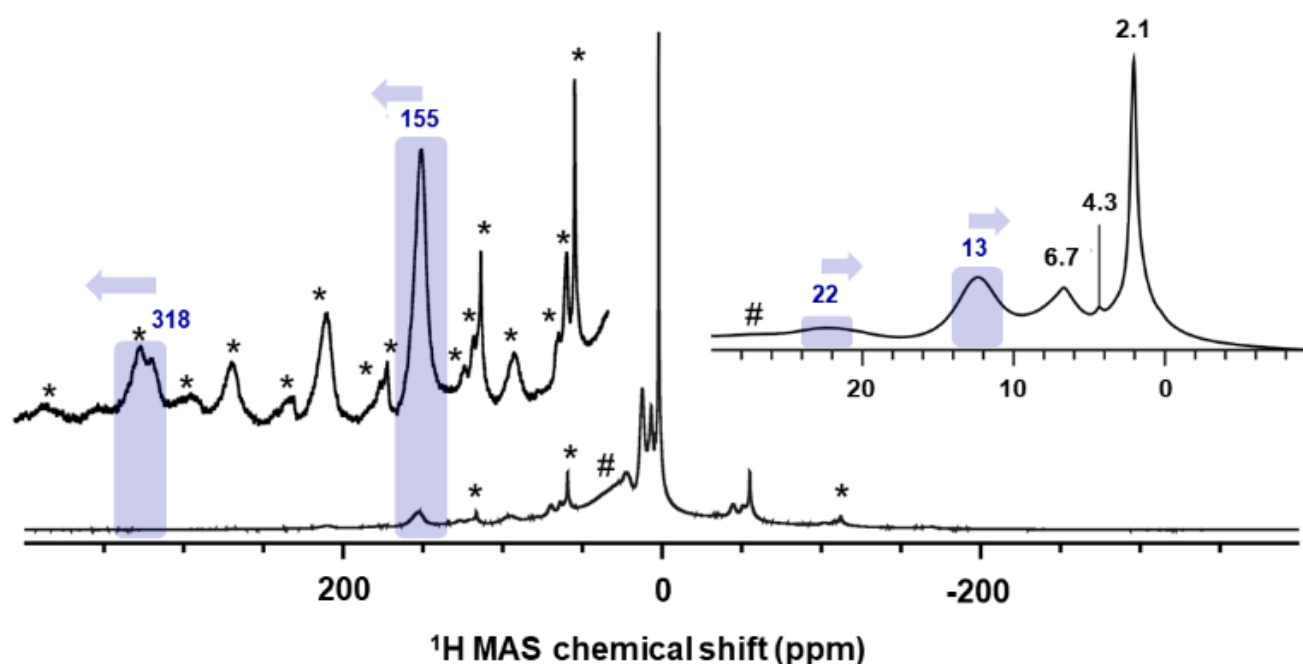


**Figure 2.** 1D relaxation-resolved  $^1\text{H}$  MAS NMR echo spectrum of **1-SiO<sub>2</sub>-1** acquired at 35 kHz MAS, 16.4 T, 0.005 s recycle delay, and a temperature of 280 K measured in the gas stream near the NMR rotor. The paramagnetic peaks are shown in blue, whereas the spinning sidebands and a background signal are indicated by “\*” and “#” symbols, respectively. The blue arrows show the shift of the peaks upon cooling to 240 K. The peaks at 2.1, 4.3, and 6.7 ppm are indicative of isolated and interacting OH groups and trace amounts of cyclopentadiene adsorbed on silica respectively.

## 2. Effect of the Cr loading

To further investigate the attribution of the various resonances to specific surface sites, we next investigated  $^1\text{H}$  MAS NMR spectra of UC-like catalysts with different Cr loadings. In the  $^1\text{H}$  MAS NMR spectrum of **1-SiO<sub>2</sub>-0.25** (0.25 wt. % Cr loading), only the two highly de-shielded resonances at 318 ppm and 155 ppm (Fig. S4) are observed. Based on our previous CO-IR investigation,[10] this material mainly consists of monomeric Cr(II) sites **I** (Fig. 1). In addition, these peaks shift down-field upon cooling and are therefore consistent with monomeric sites or potentially dimeric Cr(II) sites with weak Cr-Cr interactions. This could result from the interaction between **I** and adsorbed chromocene (site **III**). Alternatively, we could expect an interaction between some of the Cr center of **I** and nearby surface OH groups **I-OH**.

When increasing the Cr loading to 0.5 wt% (**1-SiO<sub>2</sub>-0.5**, Fig S5), two additional resonances appear at 22 ppm and 13 ppm (see Fig. 3). For **1-SiO<sub>2</sub>-1** and **1-SiO<sub>2</sub>-2**, no additional resonances appear; however, the peak at 13 ppm gains in intensity compared to the peak at 22 ppm (see Fig. 3, S6). The appearance of these less deshielded signals parallels the formation of dimeric sites such as **II** as evidenced earlier by the CO-IR investigations.[20] The slightly up-field shift upon cooling is also consistent with the presence of dimeric sites. The increase in intensity at 13 ppm at higher loading matches with the appearance of the low energy CO bands in IR, which we assigned to monomeric and dimeric Cr(III)-hydrides sites (**V** and **IV** respectively).[10]

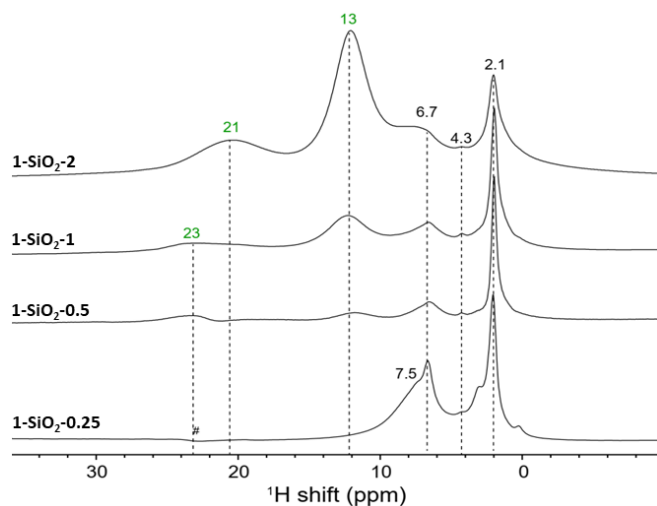


**Figure 3.** Evolution of  $^1\text{H}$  MAS NMR signal intensities in the diamagnetic region as a function of the Cr loading. A background signal in **1-SiO<sub>2</sub>-0.25** is indicated by “#”. While both peaks are absent in **1-SiO<sub>2</sub>-0.25**, the signal at 13 ppm significantly increases in intensity by increasing the Cr loading (**1-SiO<sub>2</sub>-2**).

## 3. Paramagnetic proton shifts of monomeric and dimeric molecular complexes

After having qualitatively assigned the proton shifts based on our previous proposed structures and their temperature-dependent behavior, we next calculated the respective  $^1\text{H}$  shifts to corroborate their assignment and determine the structural features of the specific surface sites. Towards this goal, we first evaluated the accuracy of the proposed calculation methodologies to predict the chemical shifts of Cp ligands by using **1** and  $[(\text{CpCr}^{\text{II}}\text{OtBu})_2]$  (**2**) as molecular models for monomeric and dimeric sites.

Experimentally, chromocene (**1**) is characterized by a peak at 325 ppm at room temperature in  $d_8$ -toluene (see Fig S7). When lowering the temperature to 253 K, the signal shifts down-field to 383 ppm (Fig. S7). The  $^1\text{H}$  shift follows an inverse temperature dependence (Fig. S10) on the temperature range from 323–238 K. Using the expression of the Fermi contact term (see section Methodology and Computational Details), the hyperfine coupling constant was fitted to 5.0 MHz (assuming  $\mathbf{g} = \mathbf{g}_e = 2$ , Fig. S10). A hyperfine coupling constant  $A$  of 3.8 MHz is predicted by DFT. From eq. 4, the  $^1\text{H}$  resonance of **1** at 293 K is expected at 301 ppm with a down-field shift to 341 ppm at 253 K. This is in good agreement with the experimentally observed behavior, indicating that this approach is suitable for estimating paramagnetic  $^1\text{H}$  shifts of monomeric chromocene-based complexes.

With the dimeric  $[(\text{CpCr}^{\text{II}}\text{OtBu})_2]$  complex **2**, we evaluate the method for  $^1\text{H}$  shift calculations in the presence of electronic spin-spin interactions. The  $^1\text{H}$  NMR spectrum of **2** shows a shift at 40 ppm corresponding to the H of the Cp ligand at room temperature in  $d_8$ -toluene. This signal moves up-field to 2 ppm ( $\delta = -38$  ppm) when cooled at 253 K (Fig. 4.A.). This effect originates from the electronic structure of complex **2**, where each  $\text{Cr}^{\text{II}}$  center is in a local high spin state ( $\mathbf{S} = 2$ , see Table S3) and the weak spin-spin interaction between the two creates five global spin states ( $\mathbf{S} = 0, 1, 2, 3$ , and 4).

These states split energetically following:

$$E_{\mathbf{S}} = \mathbf{S}(\mathbf{S} + 1)J \quad (1)$$

with  $J$  ( $\text{cm}^{-1}$ ) being the spin-spin coupling constant.[22] These states are populated according to a Boltzmann distribution at a given temperature. The coupling constant for **2** was estimated to  $-208 \text{ cm}^{-1}$  using the broken symmetry (BS) approach and the Yamagushi formula (see SI).[27] This corresponds to an energy gap of  $5.0 \text{ kJ mol}^{-1}$  between the singlet and triplet states for this complex. Thus, at 298 K, roughly 12% of **2** is in the global  $\mathbf{S} = 1$  state, while the rest (88 %) adopts a  $\mathbf{S} = 0$  state. The global spin population varies significantly with temperature (see Fig. 4A). Assuming rapid exchange between spin states compared to the NMR time scale, the effective chemical shift for dimeric sites  $\delta_{dim}$  should correspond to the Boltzmann-averaged linear combination of the Fermi contact shifts of the global spin states  $\mathbf{S}_i$ [28] as shown in equation 2:

$$\delta_{dim} = \delta_0 + \sum_{i=0}^n \delta_{FCi} \{ (N)_i / N \}$$

$$= \sigma_{Fe} - \sigma_{orb} + \sum_{i=0}^n \frac{2\pi}{\gamma_I} g\mu_B A \frac{S_i(S_i + 1)}{3k_B T} \left\{ \frac{e^{-\frac{S_i(S_i+1)J}{k_B T}}}{\sum_i e^{-\frac{S_i(S_i+1)J}{k_B T}}} \right\} \quad (2)$$

The chemical shift calculated according to eq. 7 contains a double temperature dependence: the inverse temperature dependence of the Fermi contact shift for each global spin state, as well as the population of global spin states according to the Boltzmann distribution. For simplicity reasons, the hyperfine constant  $A$  between nuclear and electronic spins was calculated for the global high spin complex and is assumed to be constant for all other spin states (see Table S6). Figure 4C displays the  $^1\text{H}$  shift curve of **2** as a combination of the Boltzmann distribution (Fig. 4A) and the individual Fermi contact shift curves (Fig. 4B) of the global spin states ( $\mathbf{S} = 0$  to 2 were considered). The predicted  $^1\text{H}$  shift curve (18 ppm, 293 K, Fig. 4C) is in reasonable agreement with the experimental data obtained in a smaller temperature interval (40 ppm, 293 K,  $d_8$ -toluene, see Fig. 4D). Although the calculated  $^1\text{H}$  chemical shift is slightly underestimated, the temperature dependence is nicely reproduced. This difference could be due to an underestimation of the  $\mathbf{S} = 1$  population, because of a slightly elongated Cr-Cr bond distance in solution for instance. Indeed, the Cr-Cr bond distance strongly impacts the spin population and thus the chemical shift behavior. Figure S12 illustrates the effect of changes in the global spin state populations on the shape of the  $^1\text{H}$  shift curve of **2** when elongating the Cr-Cr distance. As seen by the  $J$  constant, the population of higher global spin states is favored at room

temperature when the interatomic distance increases. An increase in the Cr-Cr distance by 0.25 Å (see Fig. S12) can already cause an inversion in the temperature dependence of the chemical shift curve when cooling below room temperature. From these results, we can probably attribute the small deviations between the measured and calculated chemical shifts to a small difference in the Cr-Cr distance between the crystal structure and the actual complex in solution (or on the surface).

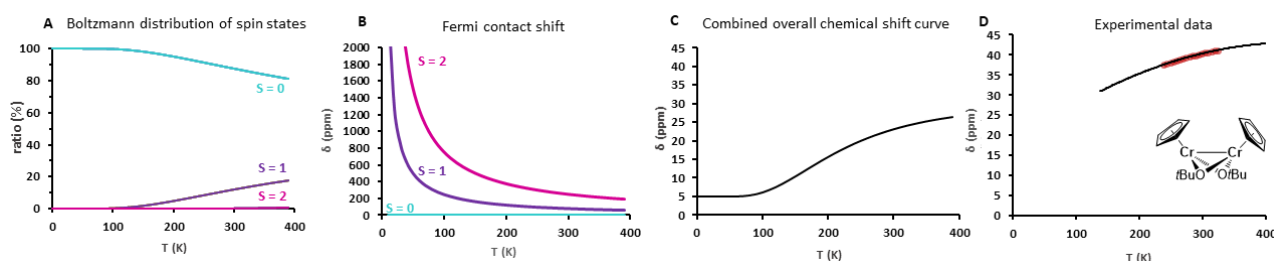


**Figure 4.** Illustration of the different contributions to the chemical shift of complex **2**. The combined overall chemical shift curve in (C) results from a linear combination of the Boltzmann distribution of spin states (A) and the Fermi contact shifts  $\delta_{FC}$  of the global spin states as visualized in (B). For **2**, a slight decrease in the chemical shift is expected while cooling below room temperature. The experimental data shown in (D) agree with the calculated  $^1\text{H}$  shift curve of (C).

The applicability of this method was then evaluated on a consistent series of dimeric complexes  $[\text{CpCrX}_{2 \text{ or } 3}]_2$  (see Table 1). For the calculations of all molecular complexes in this work, the crystal structures of the complexes were used and only the hydrogen position was optimized. The experimental trend is nicely reproduced with an increase in the  $^1\text{H}$  shift with increasing interatomic distance.

**Table 1** Experimentally measured ( $\delta_{\text{exp}}$ , benzene, 293 K) and theoretically calculated ( $\delta_{\text{calc}}$ )  $^1\text{H}$  shifts for a series of dimeric Cr complexes with increasing interatomic distances ( $d_{\text{Cr-Cr}}$ ). See Table S3-S4 for details on the calculations.

Complex	$\delta_{\text{exp}}$	$\delta_{\text{calc}}$	$d_{\text{Cr-Cr}}$
$(\text{CrCpOSi}(\text{OtBu})_3)_2$	33[1 0]	9	2.539
$(\text{CrCpOtBu})_2$	40[2 9]	18	2.632
$(\text{CpCrOtBuCl})_2$	71[3 0]	50	2.918
$(\text{CpCrCl}_2)_2$	159[ 31]	234	3.459

Overall, this methodology shows that the paramagnetic contribution to the  $^1\text{H}$  chemical shielding primarily depends on the strength of the Cr-Cr interactions. Thus, the chemical shift is a direct descriptor of the spin state of the dimer and the Cr-Cr distance can be deduced *posteriori* from the  $^1\text{H}$  shift.

#### 4. Method validation and applicability

We applied the aforescribed methodology for calculating  $^1\text{H}$  shifts of monomeric and dimeric sites on a set of paramagnetic monomeric and dimeric complexes based on 3d transition metals. For these calculations, we used the crystal structure of each complex and only optimized the proton positions (Fig. 5, see Table S3

for the references and experimental  $^1\text{H}$  chemical shifts, section S1 for the synthesis procedure of  $[\text{Cp}_2\text{Cr}]$ ,  $[(\text{Cp}_2\text{Cr}_2(\text{OSi}(\text{OtBu})_3)_2]$  and  $[(\text{Mes})_2\text{Co}]_2$ ; S2.1 for the synthesis procedure and crystallographic details of  $[(\text{Cp}_2\text{Cr}_2(\text{OSi}(\text{OtBu})_3)_3]^+$  ( $\text{Cp}_3\text{Cr}_2(\text{OSi}(\text{OtBu})_3)_4$ )). An overall good agreement ( $R^2 = 0.969$ , slope = 1.014) is obtained between experimental and theoretical data. Given the complexity of the interpretation of paramagnetic shifts, this good agreement shows that the developed methodology can be useful for structure elucidation using NMR spectroscopy of paramagnetic complexes, regardless of spin state or nuclearity. In fact, this method was also used on a reported Fe dimer,<sup>[19]</sup> where we would propose to re-assign the spectral interpretation based on the calculations (see Table. S4 and Figure S9).

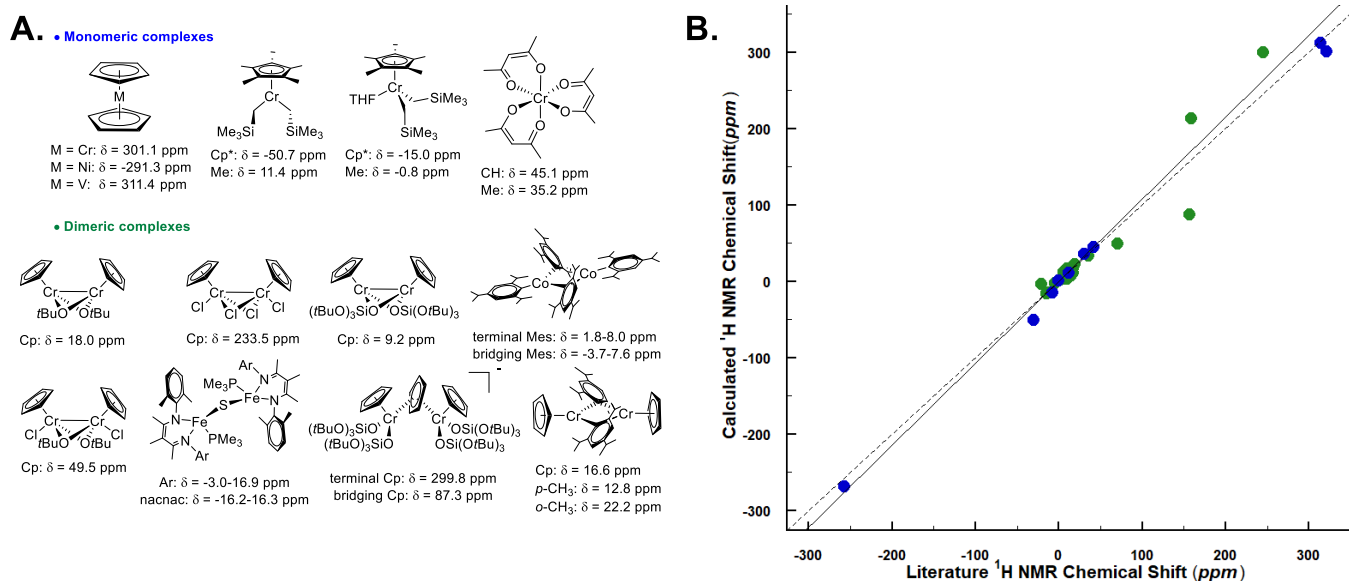


**Figure 5. A.** Monomeric and dimeric molecular complexes are included in the validation set. The proton chemical shift of the  $-\text{CH}_2-$  of  $[\text{Cp}^*\text{Cr}(\text{CH}_2\text{SiMe}_3)_2]$  and  $[\text{Cp}^*\text{Cr}(\text{CH}_2\text{SiMe}_3)_2(\text{THF})]$  is not reported Bottom) **B.** Experimental vs. calculated  $^1\text{H}$  shifts at 293 K. The blue and green dots correspond to monomeric and dimeric molecular complexes respectively. The dashed black line represents  $x = y$ . The correlation coefficient  $R^2$  for monomeric and dimeric complexes datasets are  $R^2 = 0.996$  and  $R^2 = 0.925$  respectively. For the evaluation of the choice of the basis set see the Section 4.1 in the SI.

## 5. Assigning $^1\text{H}$ chemical shifts in the UC catalyst

As stated before, in the low-Cr-loading catalyst **1-SiO<sub>2</sub>-0.25**, only two highly deshielded resonances at 318 ppm and 155 ppm are observed. According to our previous studies, this material mainly presents monomeric surface sites similar to the model site **I** ( $S = 2$ ). Calculating the proton resonance of a  $\text{CpCrOSi}$  free of interaction with the surface would predict a chemical shift of 549 ppm, while including an additional interacting oxygen ligand from a nearby Si-O-Si bridge such as in **I-OH**, predict a  $^1\text{H}$  shift at 184 ppm, which is close to the experimentally observed peak at 155 ppm as shown in Figure 6. Furthermore, these calculations predict a down-field shift to 208 ppm at 253 K, which is in the range of the experimentally observed shift from 155 ppm at 293 K to 171 ppm at 253 K for this peak. Thus, the peak at 155 ppm is best assigned to **I-OH**, an isolated, mono-grafted chromocene interacting with adjacent siloxane bridges from the silica surface (see Section 4.1.1, Fig. S12).

Note that the  $^1\text{H}$  shift of chromocene is calculated to be 301 ppm as discussed above, which is quite close to the experimentally observed peak at 318 ppm in the  $^1\text{H}$  ss-NMR spectrum (see Figure 6), likely indicating the presence of strongly adsorbed chromocene on silica. However, a similar chemical shift is expected for site **III** (dimeric Cr(II) sites with weak Cr-Cr interactions), with a  $^1\text{H}$  shift of 302 ppm for the Cp ligand located on the grafted Cr (marked in blue in Figure 6).

The nearby weakly interacting chromocene unit of site **III**, is expected at 1134 ppm assuming rapid exchange between the two Cp moieties. This signal is not observed experimentally, most likely due to the fast relaxation and the associated peak broadening (see Fig. S15 for details). Thus, the experimentally observed peak at 318 ppm is most consistent with dimeric sites such as site **III**. However, the presence of traces amount of strongly adsorbed chromocene **1** on silica cannot be excluded.

As represented in the calculated  $^1\text{H}$  shift curve of site **II** with strong Cr-Cr interactions (see Figure S13), calculations predict two peaks at 21 ppm for the “grafted part” (in green) and 15 ppm for the average of all protons of the strongly interacting chromocene unit (in orange), where all the protons can be considered equivalent (see Fig. S13). Regarding temperature dependence, calculations predict an up-field shift of 2 ppm for the peak at 23 ppm (293 K) and 1 ppm for the peak at 13 ppm (293 K) while cooling to 253 K. These findings agree with the experimental data and the up-field shift of 3 ppm (for the peak at 22 ppm) and 2 ppm (for the peak at 13 ppm) while cooling to 253 K. Details on the calculation of the chemical shift curves for site **II** are outlined in the SI Section 4.4.2.

For surface site **IV**, the protons from different Cp ligands are considered all similar with a predicted average  $^1\text{H}$  shift around 7 ppm that is almost insensitive upon temperature variation. When considering the Cp ligands separately, similar results are obtained (see Fig. S16). The fact that the intensity of the experimentally observed peak at 13 ppm increases significantly with the Cr loading (see SI section 4.4.5, Fig. S16) is consistent with the presence of an additional dimeric surface site such as **IV**, as proposed to be present in 1-SiO<sub>2</sub>-1 and 1-SiO<sub>2</sub>-2. The bridging hydride is expected at -5 ppm although not resolved experimentally likely due to low signal intensity, fast relaxation, and potential overlap with the very intense diamagnetic  $^1\text{H}$  resonances of the surface hydroxyl groups. The  $^1\text{H}$  resonance of the proposed active site structure **V** (Figure 1), which is expected at **229 ppm**, is not observed experimentally due to its low abundance (1-3 %).

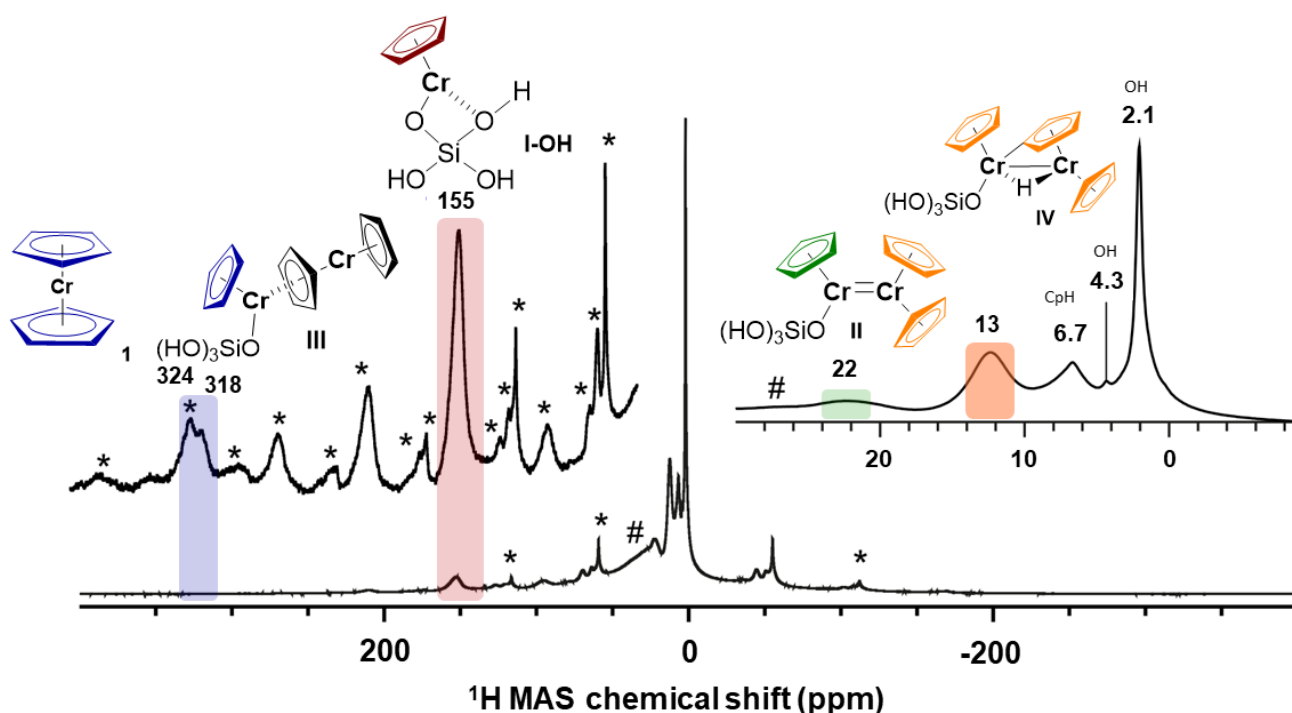


**Figure 6.**  $^1\text{H}$  MAS-NMR spectrum of **1-SiO<sub>2</sub>-1** acquired at 40 kHz MAS, 16.4 T, and a temperature of 280 K measured in the gas stream near the NMR rotor. Spinning sidebands and a background signal are indicated by “\*” and “#” symbols, respectively. The paramagnetic-shifted  $^1\text{H}$  signals are assigned to monomeric sites interacting with nearby Si-O-Si bridges from the silica surface (155 ppm, red), as well as dimeric sites with strong (**II**, 22 ppm (green) and 13 ppm (orange)) and weak (**III**, 318 ppm, blue) Cr-Cr interactions. The presence of traces amount of **1** strongly adsorbed on silica (318 ppm) cannot be excluded. C-H activated

Cr(III)-hydrides (**IV**) appear at 13 ppm and are overlapping with the strongly interacting 1 unit of site II. The signals at 2.1-4.3 ppm and 6.7-7.5 ppm in the diamagnetic region, are assigned respectively to isolated (2.1 ppm) and interacting (3.2 ppm and 4.3 ppm) surface hydroxyl groups, and trace amounts of physisorbed dicyclopentadiene (6.7-7.5 ppm).

## Conclusions

In this work, we recorded the  $^1\text{H}$  solid-state NMR of the Union Carbide catalysts at various Cr loading and developed a computational methodology to calculate the  $^1\text{H}$  NMR chemical shift of weakly coupled dimeric complexes. This method takes into account the Boltzmann-averaged over the different spin states of the Fermi contact term. Combining  $^1\text{H}$  MAS NMR signatures of monomeric and dimeric model complexes, their temperature dependence and augmented with theoretical calculations allows the assignment of monomeric and dimeric sites in the active UC-like catalyst as summarized in Figure 6 above. This method was also applied to a range of molecular paramagnetic di-nuclear complexes, illustrating its potential in assignment  $^1\text{H}$  spectra.

$^1\text{H}$  NMR investigations evidence the presence of mono-grafted sites interacting with nearby Si-O-Si bridges or surface OH groups at 155 ppm. In addition, the presence of dimeric surface sites with weak (**III**, 318 ppm) and strong Cr-Cr interactions (**II**, 22 ppm & 13 ppm) as well as the C-H activated bridging Cr(III)-hydrides (**IV**, 13 ppm) are also proposed to be present at higher loadings. Our calculations also show that trace amounts of strongly adsorbed chromocene on silica (318 ppm) cannot be excluded. The proposed active site structure **V** with a predicted  $^1\text{H}$  shift at 229 ppm is not detected experimentally, likely due to the low abundance (1-3 %) and the potential overlap with other side bands.[7, 32] Overall, this proposal is consistent with the previously published CO-IR studies, further supporting the nature of the surface species.[10] This study also demonstrates that computational approaches can now be of great help to decipher speciation in complex paramagnetic systems, by ascertaining the chemical shift assignments.

## Methodology and Computational Details

The isotropic chemical shift  $\delta$  in NMR is given by

$$\delta = \sigma_{ref} - \sigma \quad (3)$$

where  $\sigma$  represents the isotropic part of the shielding tensor, and  $\sigma_{ref}$  represents the isotropic shielding constant of the observed nucleus in a reference compound. In contrast to diamagnetic species, NMR spectra of paramagnetic systems are influenced by supplementary interactions between nuclear and electronic spins.[14, 33, 34] Therefore, the shielding constant  $\sigma$  of a nucleus in a paramagnetic environment is described by a sum of the following 3 terms:

$$\sigma = \sigma_o + \sigma_{FC} + \sigma_{PC} \quad (4)$$

where  $\sigma_o$  is the shielding of the equivalent diamagnetic molecule, and  $\sigma_{FC}$  the Fermi contact term and  $\sigma_{PC}$  the so-called pseudo-contact term. The Fermi contact shift ( $\sigma_{FC}$ ) is reversely proportional to temperature ( $T$ ) and proportional to the hyperfine coupling constant ( $A$ ) according to the following equation:

$$\sigma_{FC} = -\frac{2\pi}{\gamma_I} g\mu_B A \frac{S(S+1)}{3k_B T} \quad (5)$$

where  $\gamma_I$  is the gyromagnetic ratio of the nucleus,  $g$  is the  $g$  factor of the complex,  $\mu_B$  is the Bohr magneton and  $k_B T$  is the thermal energy. This term is the dominant contribution to the paramagnetic chemical shift of 3d-transition metal complexes and organic radicals.<sup>‡</sup>

All calculations were performed using Gaussian 09. The diamagnetic shielding constant  $\sigma_0$ , the  $g$  factor, and the hyperfine coupling constant  $A$  of Cr complexes were estimated at the B3LYP[35-38]/cc-pVTZ[39] level which was proved appropriate by Bagno and co-workers,[14] using the structures previously optimized at the B3LYP/BS1 level of theory (see SI Section 4.1) with BS1 being 6-31+G(d) for O and Cl, 6-31G(d) for C, H, and Si, and LANL2TZ/LANL2 for Cr.[40, 41] When crystal structures were available, only the positions of protons were optimized. The same approach was used for the prediction of supported monomeric and dimeric sites, where the silica surface was modeled by RO = -Si(OH)<sub>3</sub>.

Isotropic magnetic shielding tensors  $\sigma_{orb}$  was calculated using the Gauge-Independent Atomic Orbitals (GIAO) approach.[42-44] Isotropic hyperfine coupling constants  $A$ [45, 46] between nuclear and electronic spins and  $\sigma_{orb}$  were calculated as weighted average values for different sets of equivalent protons. Paramagnetic chemical shifts for monomeric sites  $\delta_{mon}$  are calculated by employing  $\sigma_0$ ,  $A$  and the molecular  $g$  factor in the equation below while using ferrocene as a reference complex ( $\sigma_{Fe}$ ) and neglecting the pseudo contact term  $\delta_{PC}$ :

$$\delta_{mon} = \delta_0 + \delta_{FC} = \sigma_{Fe} - \sigma_0 + \frac{2\pi}{\gamma_I} g\mu_B A \frac{S(S+1)}{3k_B T} \quad (6)$$

For dimeric sites presenting electronic spin-spin interactions, we account for the Boltzmann distribution of global spin states besides the Fermi contact term (see section 3 for a more detailed explanation). At first, the Fermi contact shifts are calculated for each global spin state using the  $A$  hyperfine coupling constant obtained on the high spin state. To get access to the energy splitting between global spin states ( $E = S(S+1)J$ ), spin-spin coupling constants  $J$  were calculated using the high-spin and broken symmetry (BS)[22, 27, 47] energies according to the Yamaguchi formula[14] calculated at the same level of theory used for the structure optimizations (see SI Section 1 for details).

### Author Contributions

A.N. and D.T. performed the synthesis of paramagnetic materials, Z.J.B. performed the NMR experiments, M.W. carried out the crystallographic analysis, A.N. carried out most of the calculations under the guidance of P.-A.P. P.-A.P. and C.C. designed and lead the project.

### Conflicts of interest

There are no conflicts to declare.

### Acknowledgements

Thank Dr. R. Verel, Dr. C. Gordon, and L. Lätsch for the help with NMR measurements. A.N., and D.T. are grateful to the Swiss National Foundation (SNF) for financial support of this work (grant no., 200020B\_192050 and 200021\_169134 respectively). Z.J.B. gratefully acknowledges ETH+ Project SynMatLab for financial support as well as a SNF Spark Award (grant no. CRSK-2\_190322). P.-A.P. is grateful to the ICBMS, Université Lyon 1, and the Region Auvergne Rhone Alpes for financial support. The authors would like to thank Dr. L. Perrin for fruitful discussions. The authors are grateful to the CCIR of ICBMS, PSMN, GENCI-TGCC (Grants A0100812501 and A0120813435) for providing computational resources and technical support.

## References

1. McDaniel, M.P., *Chapter 3 - A Review of the Phillips Supported Chromium Catalyst and Its Commercial Use for Ethylene Polymerization*, in *Advances in Catalysis*, B.C. Gates and H. Knözinger, Editors. 2010, Academic Press. p. 123-606.
2. Delley, M.F., et al., *Proton transfers are key elementary steps in ethylene polymerization on isolated chromium(III) silicates*. *Proceedings of the National Academy of Sciences*, 2014. **111**(32): p. 11624-11629.
3. Ashuiev, A., et al., *Molecular and supported Ti(III)-alkyls: efficient ethylene polymerization driven by the  $\pi$ -character of metal-carbon bonds and back donation from a singly occupied molecular orbital*. *Chemical Science*, 2021. **12**(2): p. 780-792.
4. Sailors, H.R. and J.P. Hogan, *History of Polyolefins*. *Journal of Macromolecular Science: Part A - Chemistry*, 1981. **15**(7): p. 1377-1402.
5. Karol, F.J., et al., *Chromocene catalysts for ethylene polymerization: Scope of the polymerization*. *Journal of Polymer Science Part A-1: Polymer Chemistry*, 1972. **10**(9): p. 2621-2637.
6. Karol, F.J. and C. Wu, *Chromocene-based catalysts for ethylene polymerization: Thermal removal of the cyclopentadienyl ligand*. *Journal of Polymer Science: Polymer Chemistry Edition*, 1974. **12**(7): p. 1549-1558.
7. Fu, S.L. and J.H. Lunsford, *Chemistry of organochromium complexes on inorganic oxide supports. 1. Characterization of chromocene on silica catalysts*. *Langmuir*, 1990. **6**(12): p. 1774-1783.
8. Fu, S.L. and J.H. Lunsford, *Chemistry of organochromium complexes on inorganic oxide supports. 2. The interactions of carbon oxides with chromocene on silica catalysts*. *Langmuir*, 1990. **6**(12): p. 1784-1792.
9. Zecchina, A., G. Spoto, and S. Bordiga, *Interaction of chromocene with the silica surface, and structure of the active species for ethene polymerization*. *Faraday Discussions of the Chemical Society*, 1989. **87**(0): p. 149-160.
10. Trummer, D., et al., *Union carbide polymerization catalysts: from uncovering active site structures to designing molecularly-defined analogs*. *Chemical Science*, 2022.
11. Theopold, K.H., *Homogeneous Chromium Catalysts for Olefin Polymerization*. *European Journal of Inorganic Chemistry*, 1998. **1998**(1): p. 15-24.
12. Theopold, K.H., et al., *Homogeneous Chromium Catalysts for Olefin Polymerization*, in *Homogeneous Transition Metal Catalyzed Reactions*. 1992, American Chemical Society. p. 591-602.
13. Schnellbach, M., F.H. Köhler, and J. Blümel, *The Union Carbide catalyst ( $Cp_2Cr + SiO_2$ ), studied by solid-state NMR*. *Journal of Organometallic Chemistry*, 1996. **520**(1): p. 227-230.
14. Rastrelli, F. and A. Bagno, *Predicting the NMR Spectra of Paramagnetic Molecules by DFT: Application to Organic Free Radicals and Transition-Metal Complexes*. *Chemistry – A European Journal*, 2009. **15**(32): p. 7990-8004.
15. Peng, L., et al., *CHAPTER 1 NMR Principles of Paramagnetic Materials*, in *NMR and MRI of Electrochemical Energy Storage Materials and Devices*. 2021, The Royal Society of Chemistry. p. 1-70.
16. Pell, A.J. and G. Pintacuda, *Broadband solid-state MAS NMR of paramagnetic systems*. *Progress in Nuclear Magnetic Resonance Spectroscopy*, 2015. **84-85**: p. 33-72.
17. Pell, A.J., G. Pintacuda, and C.P. Grey, *Paramagnetic NMR in solution and the solid state*. *Progress in Nuclear Magnetic Resonance Spectroscopy*, 2019. **111**(1873-3301 (Electronic)): p. 1-271.
18. Fernández, P., et al.,  *$^1H$  NMR Investigation of Paramagnetic Chromium(III) Olefin Polymerization Catalysts: Experimental Results, Shift Assignment and Prediction by Quantum Chemical Calculations*. *Organometallics*, 2007. **26**(18): p. 4402-4412.
19. DeRosha, D.E., et al., *A  $[2Fe-1S]$  Complex That Affords Access to Bimetallic and Higher-Nuclearity Iron-Sulfur Clusters*. *Inorganic Chemistry*, 2019. **58**(13): p. 8829-8834.
20. Trummer, D., et al., *Union carbide polymerization catalysts: from uncovering active site structures to designing molecularly-defined analogs*. *Chemical Science*, 2022. **13**(37): p. 11091-11098.

21. Borgogno, A., F. Rastrelli, and A. Bagno, *Predicting the spin state of paramagnetic iron complexes by DFT calculation of proton NMR spectra*. Dalton Transactions, 2014. **43**(25): p. 9486-9496.
22. Fontecilla-Camps, J.C., Nicolet, Yvain (Eds.), *Metalloproteins: Methods and Protocols*. 2014: Springer.
23. Polenova, T., R. Gupta, and A. Goldbourt, *Magic Angle Spinning NMR Spectroscopy: A Versatile Technique for Structural and Dynamic Analysis of Solid-Phase Systems*. Analytical Chemistry, 2015. **87**(11): p. 5458-5469.
24. Novotný, J., et al., *Crystal and Substituent Effects on Paramagnetic NMR Shifts in Transition-Metal Complexes*. Inorganic Chemistry, 2021. **60**(13): p. 9368-9377.
25. Kinney, D.R., I.S. Chuang, and G.E. Maciel, *Water and the silica surface as studied by variable-temperature high-resolution proton NMR*. Journal of the American Chemical Society, 1993. **115**(15): p. 6786-6794.
26. Korzyński, M.D., et al., *Leveraging Surface Siloxide Electronics to Enhance the Relaxation Properties of a Single-Molecule Magnet*. Journal of the American Chemical Society, 2021. **143**(14): p. 5438-5444.
27. Ferré, N., N. Guihéry, and J.-P. Malrieu, *Spin decontamination of broken-symmetry density functional theory calculations: deeper insight and new formulations*. Physical Chemistry Chemical Physics, 2015. **17**(22): p. 14375-14382.
28. Blahut, J., et al., *Monitoring Dynamics, Structure, and Magnetism of Switchable Metal–Organic Frameworks via 1H-Detected MAS NMR*. Angewandte Chemie International Edition, 2021. **60**(40): p. 21778-21783.
29. Chisholm, M.H., et al., *Dicyclopentadienyldi-tert-butoxydichromium. Preparation, properties, structure, and reactions with small unsaturated molecules*. Inorganic Chemistry, 1979. **18**(1): p. 120-125.
30. Nefedov, S.E., et al., *Antiferromagnetic complexes with the metal • metal bond: XVI. Synthesis and molecular structure of binuclear dihalogenide cyclopentadienyl-t-butylate chromium(III) complexes*. Journal of Organometallic Chemistry, 1988. **345**(1): p. 97-104.
31. Angermund, K., et al., *Cr(.eta.3-C3H5)2(.eta.5-C5H5): preparation, structure and reactions*. Organometallics, 1986. **5**(6): p. 1268-1269.
32. Fu, S.L., M.P. Rosynek, and J.H. Lunsford, *Chemistry of organochromium complexes on inorganic oxide supports. 4. Study of ethylene polymerization over chromocene on silica catalysts*. Langmuir, 1991. **7**(6): p. 1179-1187.
33. Köhler, F.H., *Paramagnetic Complexes in Solution: The NMR Approach*, in eMagRes. 2011.
34. Hrobárik, P., et al., *Density functional calculations of NMR shielding tensors for paramagnetic systems with arbitrary spin multiplicity: Validation on 3d metallocenes*. The Journal of Chemical Physics, 2007. **126**(2): p. 024107.
35. Vosko, S.H., L. Wilk, and M. Nusair, *Accurate spin-dependent electron liquid correlation energies for local spin density calculations: a critical analysis*. Canadian Journal of Physics, 1980. **58**(8): p. 1200-1211.
36. Lee, C., W. Yang, and R.G. Parr, *Development of the Colle-Salvetti correlation-energy formula into a functional of the electron density*. Physical Review B, 1988. **37**(2): p. 785-789.
37. Becke, A.D., *Density-functional thermochemistry. III. The role of exact exchange*. The Journal of Chemical Physics, 1993. **98**(7): p. 5648-5652.
38. Stephens, P.J., et al., *Ab Initio Calculation of Vibrational Absorption and Circular Dichroism Spectra Using Density Functional Force Fields*. The Journal of Physical Chemistry, 1994. **98**(45): p. 11623-11627.
39. Balabanov, N.B. and K.A. Peterson, *Systematically convergent basis sets for transition metals. I. All-electron correlation consistent basis sets for the 3d elements Sc–Zn*. The Journal of Chemical Physics, 2005. **123**(6): p. 064107.
40. Hay, P.J. and W.R. Wadt, *Ab initio effective core potentials for molecular calculations. Potentials for K to Au including the outermost core orbitals*. The Journal of Chemical Physics, 1985. **82**(1): p. 299-310.
41. Roy, L.E., P.J. Hay, and R.L. Martin, *Revised Basis Sets for the LANL Effective Core Potentials*. Journal of Chemical Theory and Computation, 2008. **4**(7): p. 1029-1031.

42. Gauss, J., *Calculation of NMR chemical shifts at second-order many-body perturbation theory using gauge-including atomic orbitals*. Chemical Physics Letters, 1992. **191**(6): p. 614-620.
43. Gauss, J., *Accurate Calculation of NMR Chemical Shifts*. Berichte der Bunsengesellschaft für physikalische Chemie, 1995. **99**(8): p. 1001-1008.
44. Wolinski, K., J.F. Hinton, and P. Pulay, *Efficient implementation of the gauge-independent atomic orbital method for NMR chemical shift calculations*. Journal of the American Chemical Society, 1990. **112**(23): p. 8251-8260.
45. Barone, V., *Electronic, vibrational and environmental effects on the hyperfine coupling constants of nitroside radicals. H<sub>2</sub>NO as a case study*. Chemical Physics Letters, 1996. **262**(3): p. 201-206.
46. Rega, N., M. Cossi, and V. Barone, *Development and validation of reliable quantum mechanical approaches for the study of free radicals in solution*. The Journal of Chemical Physics, 1996. **105**(24): p. 11060-11067.
47. Atkins, P.W., *Quanta: A Handbook of Concepts*. 2nd ed. 2010, New York: W. H. Freeman and Company.